

QCD Phase Diagrams with Charge and Isospin Axes under Heavy-Ion Collision and Stellar Conditions

K. Aryal,¹ C. Constantinou,¹ R. L. S. Farias,² and V. Dexheimer¹

¹*Department of Physics, Kent State University, Kent, OH 44243 USA*

²*Departamento de Física, Universidade Federal de Santa Maria, 97105-900 Santa Maria, RS, Brazil*

(Dated: December 22, 2024)

We investigate the phase transition from hadron to quark matter in the general case without the assumption of chemical equilibrium with respect to weak decays. The effects of net strangeness on charge and isospin fractions, chemical potentials, and temperature are studied in the context of the Chiral Mean Field (CMF) model that incorporates chiral symmetry restoration and deconfinement. The extent to which these quantities are probed during deconfinement in conditions expected to exist in protoneutron stars, binary neutron-star mergers, and heavy-ion collisions is analyzed quantitatively via the construction of 3-dimensional phase diagrams.

I. INTRODUCTION

Recent works have discussed the possible similarities between the conditions in energetic astrophysical environments, such as protoneutron stars, core-collapse supernovae, and neutron-star binary mergers, to those present in heavy-ion collisions (HICs) [1, 2]. These similarities are consequences of the high temperatures (compared to the Fermi temperature) achieved in these phenomena that, unlike in the case of chemically-equilibrated neutron stars, cannot be ignored. In particular, the temperature in protoneutron stars can be as high as 30 – 40 MeV [3, 4] and in mergers it can exceed 50 MeV or even reach 100 MeV [5, 6]. However, contemporary simulations [7] indicate that neutron-star mergers cannot attain the large charge fractions of close to $Y_Q = 0.4$ produced in HICs (eg. for Au-Au and Pb-Pb) and supernovae [8, 9]. This is a new feature, as before the advent of compact star mergers, all known astrophysical systems out of chemical equilibrium were newly formed and, therefore, still contained a significant amount of protons from the original heavy nuclei in the progenitors. As a result of the recent multi-messenger signals, together with more refined HIC calculations that allow for large chemical potential fluctuations [10], it became important to study hot and dense matter in a large range of charge fractions.

Phase diagrams for high energy matter (or Quantum Chromo Dynamics - QCD - phase diagrams) are usually only depicted in two dimensions, temperature and baryon number density/chemical potential or temperature and isospin number density/chemical potential. The latter are interesting due to the fact that lattice QCD results are not afflicted by the sign problem at finite isospin chemical potential μ_I , as long as the baryon chemical potential μ_B remains zero. When $\mu_B \neq 0$ or, equivalently, when there is a difference in the number of particles and anti-particles in the system, first-principle methods such as non-perturbative lattice QCD simulations cannot be performed [11–13].

Finite μ_I and zero μ_B calculations have recently received a lot of attention due to their relevance to

HICs [14], compact stars [15–17] and even to the evolution of the early Universe [18]. These calculations can be used to verify the reliability of the predictions of effective models of QCD when compared to first principle results [19–25]. In the case of QCD at finite isospin density, the first lattice simulations were done in Refs. [26, 27] using unphysical pion masses and/or unphysical flavor content. The results from these first simulations were in qualitative agreement with the different approaches to QCD [28–61]. Other interesting approach that is applied to study QCD at finite isospin chemical potential is based in holographic models [62–68]. More recently, lattice QCD results for finite isospin density were performed using an improved lattice action with staggered fermions at physical quark and pion masses [69–72], their predictions being in very good agreement with the results obtained from updated chiral perturbation theory [73–75] and NJL models [76–78].

Another issue raised in the literature is the manner in which strangeness can affect QCD phase diagrams. Ref. [79] has recently studied this for the particular case of isospin symmetric matter using functional renormalization theory. However, this is not a new topic, as the pioneering work presented in Refs. [80, 81] discussed a mixture of phases created when quark matter containing strange matter and hadronic matter containing anti-strange matter coexist in the 1980s, a conjecture first suggested in Refs. [82, 83]. Lattice QCD calculations have also studied the effects of a non-zero strange chemical potential in, for example, the curvature of the chiral pseudo-critical line [84, 85]. In this work, we consider two scenarios. In one of them, there is no restriction on strangeness, assuming that chemical equilibrium with respect to the weak force has already been achieved, in which case there is no need to define a strange chemical potential. In the other case, net strangeness is assumed to not yet have had enough time to be produced, in which case the strange chemical potential must be numerically determined in each phase to produce a zero net-strangeness fraction.

When the baryon chemical potential is finite, the usual practice in the literature has been to construct 2-

dimensional phase diagrams (with temperature on the other axis) either in weak-chemical equilibrium, referring to fully-evolved neutron star matter, or in an isospin-symmetric configuration, referring to matter created in relativistic HICs. In this work, we examine the behavior of the deconfinement coexistence line in 3-dimensional phase diagrams as a function of either the (hadronic and quark) charge fraction Y_Q or the isospin fraction Y_I (with temperature and baryon chemical potential/free energy completing our coordinate system). Note that Y_Q is the variable usually employed in equations of state for astrophysical applications, while Y_I is more commonly used in HIC applications. The relation among the two quantities is trivial only when net strangeness is absent. Our calculations and discussion extend to phase diagrams in which the charge and isospin fractions are replaced by the corresponding chemical potentials, both at zero and non-zero net strangeness. As pointed out in Ref. [86], it is important to understand which plane of the QCD phase diagram is being probed, eg. in the HIC Beam Energy Scan experiment, as the traditional critical point for isospin-symmetric matter without strangeness constraints may never be reached in the experiment.

II. FORMALISM

A. The CMF model

In order to construct our phase-diagrams, we make use of the Chiral Mean Field (CMF) description. It is based on a nonlinear realization of the $SU(3)$ sigma model and constructed in such a way that chiral invariance is restored at large temperatures and/or densities. In its present version, it contains hadronic, as well as quark degrees of freedom¹, and its Lagrangian density is given by [89, 90]:

$$\mathcal{L} = \mathcal{L}_{\text{Kin}} + \mathcal{L}_{\text{Int}} + \mathcal{L}_{\text{Self}} + \mathcal{L}_{\text{SB}} - U, \quad (1)$$

where \mathcal{L}_{Kin} is the kinetic energy density of hadrons and quarks. The remaining terms are:

$$\begin{aligned} \mathcal{L}_{\text{Int}} &= - \sum_i \bar{\psi}_i [\gamma_0 (g_{i\omega} \omega + g_{i\phi} \phi + g_{i\rho} \tau_3 \rho) + M_i^*] \psi_i, \\ \mathcal{L}_{\text{Self}} &= \frac{1}{2} (m_\omega^2 \omega^2 + m_\rho^2 \rho^2 + m_\phi^2 \phi^2) \\ &\quad + g_4 \left(\omega^4 + \frac{\phi^4}{4} + 3\omega^2 \phi^2 + \frac{4\omega^3 \phi}{\sqrt{2}} + \frac{2\omega \phi^3}{\sqrt{2}} \right) \\ &\quad - k_0 (\sigma^2 + \zeta^2 + \delta^2) - k_1 (\sigma^2 + \zeta^2 + \delta^2)^2 \\ &\quad - k_2 \left(\frac{\sigma^4}{2} + \frac{\delta^4}{2} + 3\sigma^2 \delta^2 + \zeta^4 \right) - k_3 (\sigma^2 - \delta^2) \zeta \end{aligned}$$

$$- k_4 \ln \frac{(\sigma^2 - \delta^2) \zeta}{\sigma_0^2 \zeta_0}, \quad (2)$$

$$\mathcal{L}_{\text{SB}} = -m_\pi^2 f_\pi \sigma - \left(\sqrt{2} m_k^2 f_k - \frac{1}{\sqrt{2}} m_\pi^2 f_\pi \right) \zeta, \quad (3)$$

$$\begin{aligned} U &= (a_o T^4 + a_1 \mu_B^4 + a_2 T^2 \mu_B^2) \Phi^2 \\ &\quad + a_3 T_o^4 \ln (1 - 6\Phi^2 + 8\Phi^3 - 3\Phi^4). \end{aligned} \quad (3)$$

Here, \mathcal{L}_{Int} represents the interactions between baryons (and quarks) mediated by the vector-isoscalar mesons ω and ϕ (strange quark-antiquark state), the vector-isovector ρ , the scalar-isoscalars σ and ζ (strange quark-antiquark state), and the scalar-isovector δ . $\mathcal{L}_{\text{Self}}$ describes the self-interactions of the scalar and vector mesons. The chiral symmetry breaking term responsible for producing the masses of the pseudoscalar mesons is given by \mathcal{L}_{SB} . U is the effective potential for the scalar field Φ and depends on the temperature and the baryon chemical potential. It is analogous to the Polyakov loop in the PNJL approach [91, 92]. The index i runs over the baryon octet and the three light quarks. Leptons are not included in this calculation, since they are not present in HIC initial conditions and are not in chemical equilibrium with the rest of the system in the astrophysical scenarios we discuss.

The coupling constants of the hadronic part of the model are given in Ref. [93]. They were fitted to reproduce the vacuum masses of baryons and mesons, nuclear saturation properties (density $\rho_0 = 0.15 \text{ fm}^{-3}$, binding energy per nucleon $B/A = -16 \text{ MeV}$, compressibility $K = 300 \text{ MeV}$), symmetry energy ($E_{\text{sym}} = 30 \text{ MeV}$ with slope $L = 88 \text{ MeV}$), and reasonable values for the hyperon potentials ($U_\Lambda = -28.00 \text{ MeV}$, $U_\Sigma = 5 \text{ MeV}$, $U_\Xi = -18 \text{ MeV}$). The predicted critical point for the nuclear liquid-gas phase transition of isospin symmetric matter lies at $T_c = 16.4 \text{ MeV}$, $\mu_{B,c} = 910 \text{ MeV}$. The vacuum expectation values of the scalar mesons are constrained by reproducing the pion and kaon decay constants.

As a result of their interactions with the mean field of mesons and the field Φ , the baryons and the quarks acquire (Dirac) effective masses, which have the form:

$$\begin{aligned} M_B^* &= g_{B\sigma} \sigma + g_{B\delta} \tau_3 \delta + g_{B\zeta} \zeta + M_{0_B} + g_{B\Phi} \Phi^2, \\ M_q^* &= g_{q\sigma} \sigma + g_{q\delta} \tau_3 \delta + g_{q\zeta} \zeta + M_{0_q} + g_{q\Phi} (1 - \Phi), \end{aligned} \quad (4)$$

where the bare masses are $M_0 = 150 \text{ MeV}$ for nucleons, 354.91 MeV for hyperons, 5 MeV for up and down quarks, and 150 MeV for strange quarks (see Ref. [93] for the coupling constants in the quark sector). Notice that for vanishing values of Φ , M_q^* is large, which suppresses the quarks. Conversely, values of Φ close to 1 suppress the hadrons. In this sense, Φ acts as an order parameter for deconfinement.

The coupling constants of the quark sector are fitted to lattice data and to expectations from the phase diagram. The lattice data include (1) the location of the first-order phase transition and the pressure functional $P(T)$ at $\mu_B = 0$ for pure gauge [92, 94] and (2)

¹ Note that an alternative version of the CMF model includes in addition the chiral partners of the baryons and gives the baryons a finite size [87, 88].

the crossover pseudo-critical temperature and susceptibility $d\Phi/dT$ at vanishing chemical potential, together with the location of the (T, μ_B) critical end-point for zero net-strangeness isospin-symmetric matter [95]. The phase diagram expectations include a continuous first-order phase-transition line that terminates on the zero-temperature axis at four times the saturation density of chemically-equilibrated and charge-neutral matter. See Ref. [93, 96] for a detailed description of the effects of deconfined quarks inside neutron and protoneutron stars within the CMF model.

Note that the CMF description allows for the existence of soluted quarks in the hadronic phase and soluted hadrons in the quark phase at finite temperature. This feature becomes more prominent with increasing temperature and is required in order to reproduce a crossover transition at very large temperatures [97]. Despite this, quarks always have the dominant contribution in the quark phase, and hadrons in the hadronic phase.

In this work, we choose to only show our phase diagrams until $T = 160$ MeV, a little bit below the critical temperature $T_c = 167$ MeV predicted by the current parametrization of the model for zero net-strangeness isospin-symmetric matter. This is done for two different reasons. First, our critical point position was fitted and any modification to it would not affect the qualitative conclusions of our work. Second, we want to keep the discussion entirely general and the inclusion of a "special" feature, such as the critical point, will detract from our goals. In addition, the CompOSE [98] repository contains equation of state tables that go up to $T = 160$ MeV, so all of our results could be reproduced as soon as our tables are uploaded to their website. So far, only the hadronic version of our tables are available online [99], but complete ones with quarks will be available soon.

B. Useful Relations

We are interested in systems that are in equilibrium with respect to the strong and electromagnetic interactions, therefore, baryon number B and electric charge Q are fixed. In some of the cases we study, chemical equilibrium is not attained because weak interactions operate over much longer timescales (then the time scale of the system), introducing an extra condition of zero net strangeness S . The above conserved quantities correspond to our three independent chemical potentials μ_B , μ_Q , and μ_S . The total chemical potential μ_i of each fermionic species i can be expressed as a linear combination of these, according to:

$$\mu_i = Q_{B,i} \mu_B + Q_i \mu_Q + Q_{S,i} \mu_S. \quad (5)$$

The conventions we adopt for the values of the Q 's for the baryon octet and the three light quark species are given in Table I of Appendix A, followed by the resulting chemical potentials of the various species. Note that we consider the strangeness of particles to be positive in our notation,

otherwise, all strangeness related quantities would have to have their signs reversed. For the purposes of our calculations, it is more convenient to work with fractions, the charge fraction being the amount of charged baryons and quarks over the total amount of baryons and quarks:

$$Y_Q = \frac{Q}{B} = \frac{\sum_i Q_i n_i}{\sum_i Q_{B,i} n_i} = \frac{n_Q}{n_B^0}, \quad (6)$$

where n_i is the number density of each baryon/quark and n_Q is the charge density. Note that $n_B^0 = \sum_i Q_{B,i} n_i$ is not the same as the baryon number density n_B , as the latter comes from the derivative of the pressure with respect to the baryon chemical potential and, therefore, also contains a contribution from the potential $U(\Phi)$ when quarks are present (see Eq. (3)). For low temperatures, this contribution can be safely ignored on the hadronic side of the phase-coexistence region, where Φ is approximately zero and, thus, $n_B^0 \simeq n_B$. Furthermore, we can insert the Gell-Mann-Nishijima relation [100]:

$$Q_i = Q_{I,i} + \frac{1}{2}Q_{B,i} - \frac{1}{2}Q_{S,i}, \quad (7)$$

where $Q_{I,i}$ is the isospin of particle i , in the definition of charge density Eq. (6) to obtain:

$$\begin{aligned} n_Q &= \sum_i (Q_{I,i} + \frac{1}{2}Q_{B,i} - \frac{1}{2}Q_{S,i}) n_i, \\ &= n_I + \frac{1}{2}n_B^0 - \frac{1}{2}n_S, \end{aligned} \quad (8)$$

where we have also used the definitions of the isospin density $n_I = \sum_i Q_{I,i} n_i$ and strangeness density $n_S = \sum_i Q_{S,i} n_i$. Dividing Eq. (8) by n_B^0 and defining $Y_I = n_I/n_B^0$ and $Y_S = n_S/n_B^0$, results in:

$$Y_Q = Y_I + \frac{1}{2} - \frac{1}{2}Y_S, \quad (9)$$

so we can finally write:

$$Y_I = Y_Q - \frac{1}{2} + \frac{1}{2}Y_S, \quad (10)$$

as a way to calculate the isospin fraction in our formalism.

Combining Eqs. (5) and (7) gives:

$$\begin{aligned} \mu_i &= Q_{B,i} \mu_B + (Q_{I,i} + \frac{1}{2}Q_{B,i} - \frac{1}{2}Q_{S,i}) \mu_Q + Q_{S,i} \mu_S, \\ &= Q_{B,i} (\mu_B + \frac{1}{2} \mu_Q) + Q_{I,i} \mu_Q + Q_{S,i} (\mu_S - \frac{1}{2} \mu_Q), \\ &= Q_{B,i} \mu'_B + Q_{I,i} \mu_I + Q_{S,i} \mu'_S. \end{aligned} \quad (11)$$

A comparison of the above with Eq. (5) reveals that our formalism is equivalent to another in which the isospin is fixed, leaving the isospin chemical potential as the independent chemical potential (together with μ_B and μ_S), provided we define the following new variables:

$$\mu'_B = \mu_B + \frac{1}{2} \mu_Q \quad \text{and} \quad \mu'_S = \mu_S - \frac{1}{2} \mu_Q. \quad (12)$$

In this way, the chemical potentials correspond, $\mu_I = \mu_Q$, and no modifications to our formalism and numerical codes are required to show isospin fractions and isospin chemical potentials (as long as Eq. (5) and Eq. (11) are used). To the best of our knowledge, this has never been discussed before. The expressions for the chemical potential of each particle included in the model derived using Eq. (5) or Eq. (11) are given in Appendix A.

It is also convenient to define a Gibbs free energy per baryon (henceforth called simply free energy) of the system, a quantity that is always the same on both sides of a first-order phase transition. In our case (when, besides baryon number, charge fraction and strangeness fraction are being fixed), it is:

$$\tilde{\mu} = \mu_B + Y_Q \mu_Q + Y_S \mu_S. \quad (13)$$

Note that the free energy will be equal to the baryon chemical potential only in the particular cases of zero charge fraction or zero charge chemical potential and zero strange fraction or strange chemical potential. This is the case in the modeling of the typical examples of deleptonized cold neutron stars (charge neutral in chemical equilibrium $Y_Q = 0$ and with no constraint on net strangeness $\mu_S = 0$) and relativistic HICs (no net isospin $\mu_Q = 0$ and no net strangeness $Y_S = 0$).

Eq. (13) was derived and discussed in detail in the Appendix D of Ref. [101] for the particular case in which net strangeness is not constrained (which implies $\mu_S = 0$). It can be derived either by a Legendre transformation of the grand-potential or by taking the derivative of minus the grand-potential with respect to the baryon number, giving:

$$\tilde{\mu} = \sum_i \mu_i n_i / n_B^0. \quad (14)$$

Substituting μ_i from Eq. (5) in Eq. (14) results in Eq. (13). Alternatively, following the equivalent isospin formalism and replacing μ_i from Eq. (11) in Eq. (14) leads to:

$$\tilde{\mu} = \mu'_B + Y_I \mu_I + Y_S \mu'_S. \quad (15)$$

III. RESULTS

A. Non-Strange Matter $Y_S = 0$

We start by discussing phase diagrams showing the deconfinement coexistence line calculated within the CMF model for temperatures in the range 0–160 MeV, charge fractions in the range 0–0.5, and the corresponding baryon chemical potentials μ_B or free energies $\tilde{\mu}$. In this subsection, the strange chemical potential is determined numerically at each point in each diagram in order to produce a zero net strangeness $Y_S = 0$ in each phase. Having $Y_Q = 0$ means that there is no net charge in the system even though the presence of charged particles is not prohibited insofar as the sum of their charges is zero. Having $Y_Q = 0.5$ corresponds to the situation where the

total baryon number of the system is twice as large as its net charge. For matter with no net strangeness at zero temperature, the case of $Y_Q = 0$ is equivalent to having just neutrons or two times more d-quarks than u-quarks, whereas $Y_Q = 0.5$ corresponds to having equal amounts of protons and neutrons or d- and u-quarks. At finite temperature, there can be hyperons and s-quarks present when requiring no net strangeness, as long as the difference between the number of strange particles and strange antiparticles is zero.

Note that for non-strange matter Eq. (13) simplifies to:

$$\tilde{\mu} = \mu_B + Y_Q \mu_Q. \quad (16)$$

This is the case for matter produced in HICs, where there is no time for strangeness to emerge. The free energy of the deconfinement coexistence line is determined by finding a jump in the deconfinement order parameter Φ . As shown in the bottom panel of Fig. 1, the deconfinement free energy increases as a function of Y_Q . This behavior is related to the softening of nuclear matter with increased net charge (e.g. equal numbers of neutrons and protons), the effect being stronger for hadronic matter. A softening of the equation of state (pressure vs. energy density) of hadronic matter corresponds to an increase in pressure at a given free energy (with respect to the quark phase), therefore, extending the hadronic phase to larger free energies.

The free energy is the same on both sides of the deconfinement coexistence line (shown in the bottom panel of Fig. 1), but the baryon chemical potential is not. This is evident in a comparison of the top left (hadrons) to the top right (quarks) panel of the same figure. The difference stems from the fact that the baryon chemical potential is calculated from the free energy using the charged chemical potential, which is different on either side of the phase transition (the reason for which will be discussed in the following). In addition, when comparing the top left panel with the bottom one, we find a reasonable difference for all cases corresponding to $\mu_B \neq \tilde{\mu}$ in Eq. (16), that is, for all Y_Q other than 0 and 0.5 (when $\mu_Q = 0$).

The difference is much smaller between the top right panel of Fig. 1 and the bottom one, as the charged chemical potential μ_Q is always small in the quark phase. This has already been shown in Fig. 3 of Ref. [93] for the particular case of chemically equilibrated matter (with and without trapped neutrinos). Here, we extend this discussion to matter out of chemical equilibrium. A comparison of the left and right panels of Fig. 2 demonstrates that the hadronic side reaches much larger absolute values of μ_Q than the quark phase for small charge fractions (corresponding to the more negative μ_Q 's). This can be easily understood in the case of zero temperature. $Y_Q = 0$ means having only neutrons (and no protons), which requires a very large difference in their chemical potentials μ_i that differ only by μ_Q (as shown in the equations of Appendix A). In the quark phase, $Y_Q = 0$ implies having twice the amount of d-quarks than u-quarks, a much

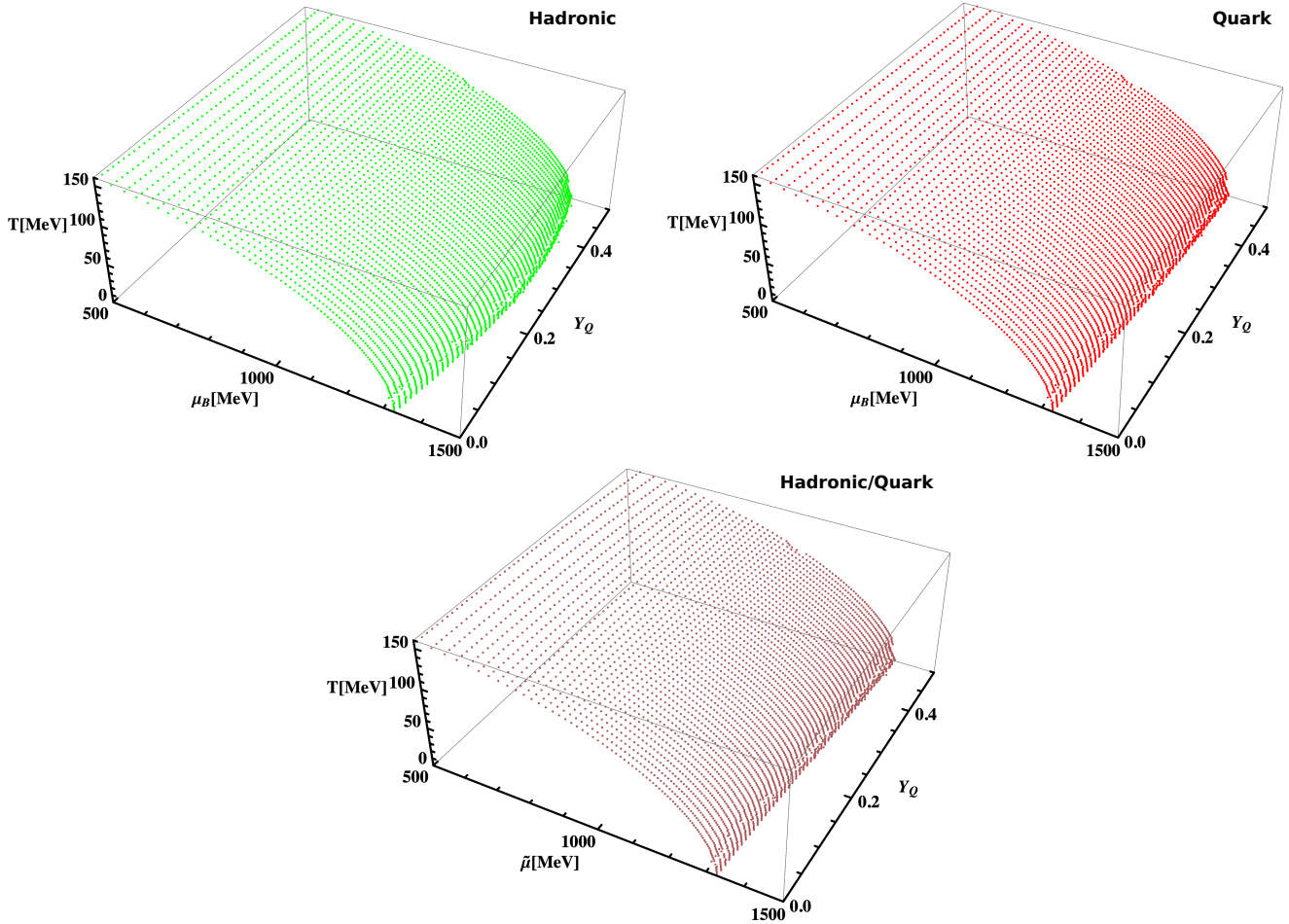


Fig. 1: Top panels: The temperature T vs. baryon chemical potential μ_B vs. charge fraction Y_Q phase diagram for non-strange matter $Y_S = 0$ on the hadronic side of the deconfinement phase transition (left panel) and on the quark side (right panel). Bottom panel: The temperature T vs. free energy $\tilde{\mu}$ vs. charge fraction Y_Q phase diagram for non-strange matter either on the hadronic or quark side of the deconfinement phase transition. All curves were calculated varying the charge fraction between $Y_Q = 0$ and $Y_Q = 0.5$.

more balanced case that requires a smaller μ_i difference and, therefore, a smaller μ_Q absolute value.

In the case of Fig. 2 (unlike Fig. 1), the bottom panels are always different from each other, because the charged chemical potential itself is discontinuous across the first-order phase transition. Analyzing separately the hadronic (left) side of the coexistence line in Fig. 2, it can be seen that the curves in the top and bottom panels are always different, except on the upper and lower boundaries of μ_Q .

We show phase diagrams as functions of charge fraction because this is common practice in astrophysics, where the requirement of charge neutrality implies $Y_{\text{lepton}} = Y_Q$. There is no corresponding general equality for the lepton chemical potential: the relation $\mu_{\text{lepton}} = -\mu_Q$ is only valid in the special case of chemical equilibrium, which is only established in deleptonized cold neutron stars.

Similar figures to Figs. 1 and 2 are presented in Appendix B for the equivalent scenario of fixed isospin frac-

tion. For non-strange matter, Eq. (10) reduces simply to $Y_I = Y_Q - 0.5$, and therefore the changes in both figures are trivial. More details are given in the Appendix.

B. Strange matter $Y_S \neq 0$

In this subsection, we compactify the temperature and only show results for $T = 0$ MeV and $T = 160$ MeV (corresponding to the two temperature extremes in our previous figures) in order to be able to make more quantitative statements. Full 3-dimensional strange phase diagrams are available upon request. In addition to quantities shown in the preceding subsection (for matter with net strangeness constrained to zero) using the same colors, we now display strange matter results in black for comparison. By strange matter, we mean matter in which there is no constraint on net strangeness and therefore, no strange chemical potential, $\mu_S = 0$. For $T = 0$ MeV,

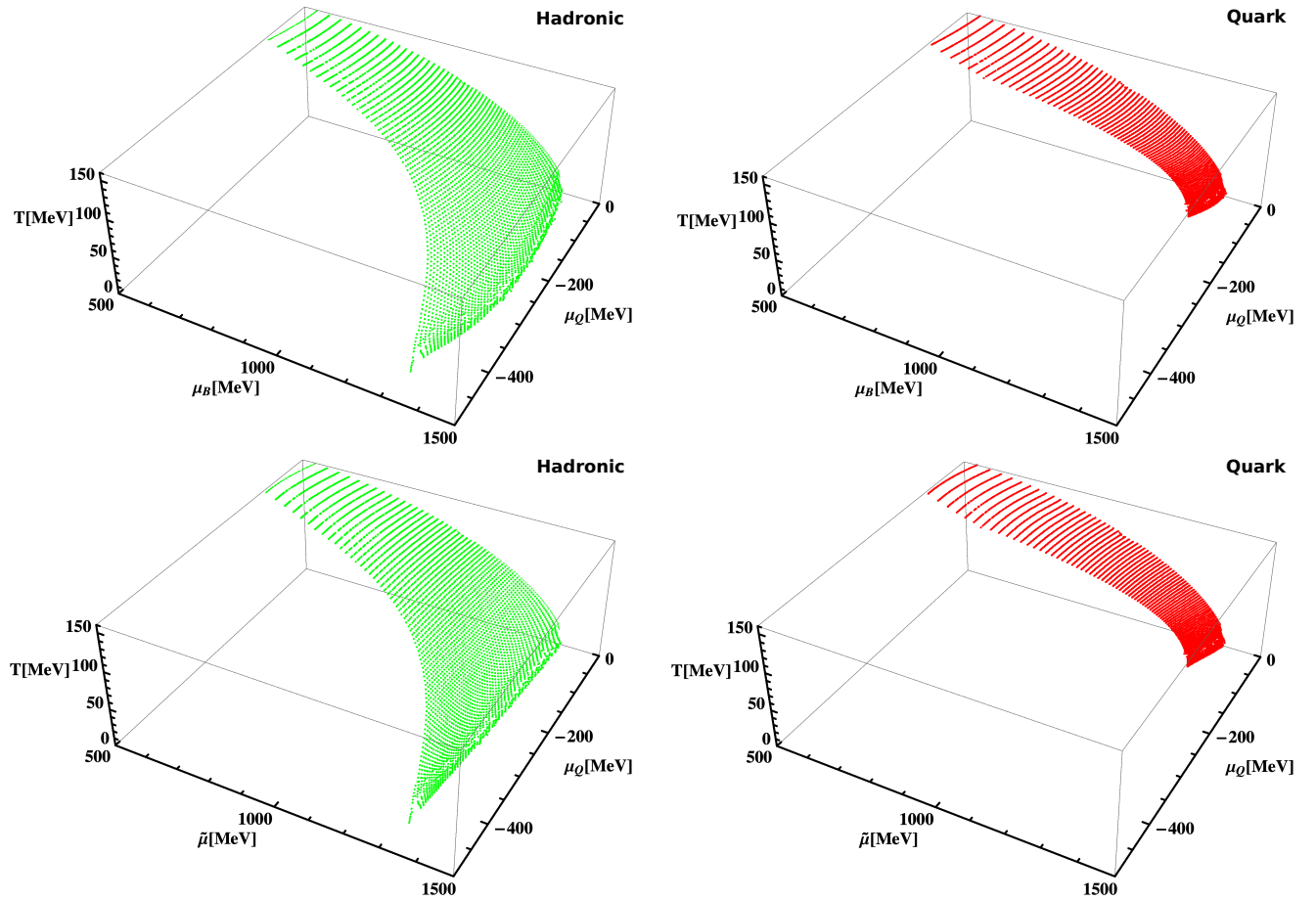


Fig. 2: Same as Fig. 1 but showing the charged chemical potential μ_Q . The separate bottom panels show the hadronic (left panel) and quark (right panel) sides of the deconfinement phase transition

no significant difference in the position of the deconfinement line with respect to the baryon chemical potential or the free energy is expected due to allowing for nonzero strangeness. This is because, in this case, in our formalism, only a few Λ 's and Σ^- 's are present around the deconfinement free energy (and no strange quarks) and only at small charge fractions. This is illustrated in the difference between the brown dashed line and the black dashed line in the upper left panel of Fig. 3. The strange black dashed line being at a larger $\tilde{\mu}$ than the non-strange brown dashed line is a consequence of the hyperons softening hadronic matter when they appear (for low charge fraction) and pushing the phase transition to larger values of $\tilde{\mu}$.

The difference in the position of the deconfinement line with respect to the baryon chemical potential is related to the presence of strange particles, which modify the charged chemical potential relative to the zero-strangeness case (Eq. (13) reduces once more to Eq. (16) for $\mu_S = 0$). As a consequence, as shown in the green vs. black stars in the same panel, μ_B on the hadronic side is lower around intermediate charge fractions for the strange case. This is a combination of μ_Q being lower in

absolute value for low and intermediate values of Y_Q (see bottom left panel of Fig. 3) for strange matter and the fact that μ_Q is multiplied by Y_Q in Eq. (16). As for the quark side of the phase transition, μ_Q is always small in absolute value (see again bottom left panel of Fig. 3), so μ_B behaves very similarly to $\tilde{\mu}$, as seen when comparing black and red dot dashed lines in the top left panel of Fig. 3.

For large temperatures, strangeness generates much larger effects and the phase transition itself is very weak (particularly for the case without net strangeness), becoming very similar to a crossover. The former translates to a significant difference in the position of the black vs. colored lines in the top right panel of Fig. 3: the strange black dashed line for $\tilde{\mu}$ resides about 40 MeV higher than the non-strange dashed pink one. For $T=0$, this difference is $\lesssim 5$ MeV. This shift is a consequence of the fact that at large temperatures the presence of strangeness-carrying particles is enhanced at all charge fractions, thus softening the quark equation of state (relative to the hadronic one) around deconfinement.

To discuss the baryon chemical potential, we first note that at this large temperature, which is very close to the

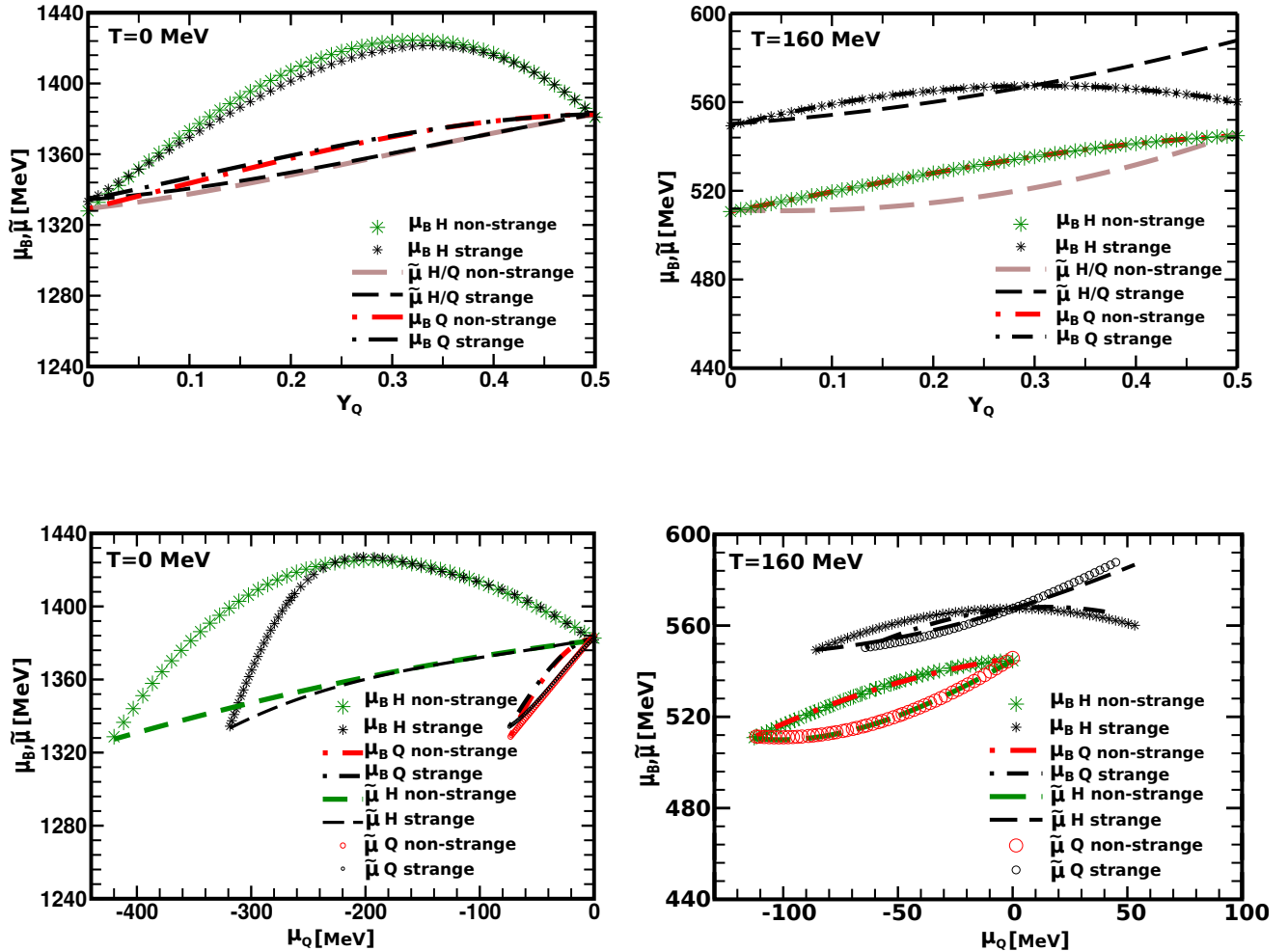


Fig. 3: Equivalent to Fig. 1 (top panels) and Fig. 2 (bottom panels) but only showing results for 0 (left panels) and 160 MeV (right panels) temperatures. Green, red and brown lines (all grey in black and white print) show results already discussed for non-strange matter, while black lines show new results for strange matter.

critical point, the hadronic side and quark side of the deconfinement phase transition are nearly identical. The difference in the position of μ_B with respect to $\tilde{\mu}$ has to do with the fact that, once again, the charged chemical potential difference also needs to be accounted for. When looking at the black stars and dot-dashed line still in the upper right panel of Fig. 3, we find that it is lower in comparison with the dashed line for $\tilde{\mu}$ (than in the colored non-strange case). This has to do with the fact that μ_Q is lower in absolute value and even positive for some large charge fractions when strangeness is included (see black lines in the right bottom panel of Fig. 3).

Fig. 4 shows the effects of strangeness on the baryon chemical potential and the free energy as a function of the isospin fraction Y_I . Now, when net strangeness is non-zero (black curves), the left panel in this figure is not simply a constant horizontal shift from the Y_Q shown in the

previous figure, but a shift that, according to Eq. (10), depends on the strangeness fraction and, therefore, is different for every point. The horizontal shift is always positive and larger for low Y_I/Y_Q at zero temperature, where there is more net strangeness. At $T = 160$ MeV, the black lines in the right panel of Fig. 4 show that the horizontal shift is always positive and substantial for all Y_I/Y_Q , as, in this case, net strangeness is always present.

Note that in Fig. 4 we do not show bottom panels for isospin chemical potential, as they would be identical to the charged chemical potential bottom panels of Fig. 3. In addition, if instead of using Eq. (10) to calculate Y_I , we had rewritten our numerical code to run for fixed isospin fraction from -0.5 to 0, we would have obtained the same results as shown in Fig. 4 but with an extra piece on the left and a missing piece on the right side of our finite temperature panel, a consequence again of the non-trivial

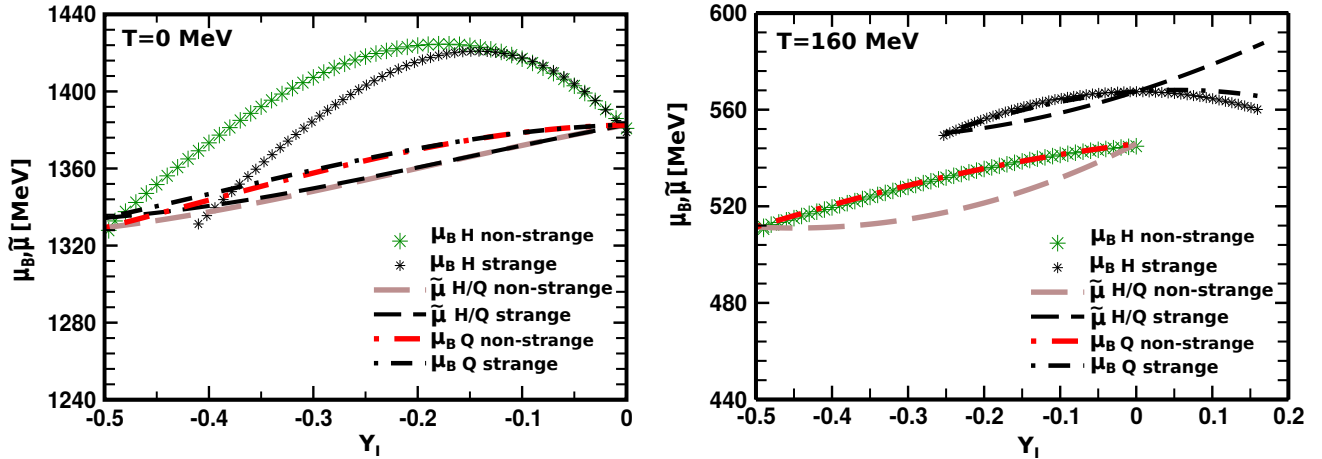


Fig. 4: Same as the top panels of Fig. 3 but showing the isospin fraction Y_I . Equivalent isospin chemical potential panels would be exactly like the charged chemical potential bottom panels of Fig. 3.

Y_Q to Y_I shift.

IV. DISCUSSION AND CONCLUSIONS

We present, for the first time, a comprehensive study of the effects of (hadronic and quark) charge fraction and isospin fraction on the deconfinement to quark matter using the CMF model. We derive model-independent relations among these quantities and discuss how they are affected by the presence of net strangeness. We also discuss the relation between the respective isospin and charge chemical potentials. This discussion is extremely timely as, historically, the heavy-ion collision community has modeled their systems in terms of fixed isospin fraction, while the astrophysical community has modeled it in terms of charge fraction (equal to the electron fraction when muons are not included), whereas now these communities are working together to understand the hot and dense matter generated in neutron star mergers and in low energy heavy-ion collisions.

Our goal has been to obtain a quantitative description of the manner in which charge fraction and isospin fraction change the position of deconfinement coexistence line with respect to temperature and baryon chemical potential or Gibbs free energy per baryon. To that end, we have built 3-dimensional phase diagrams for matter that possesses no net strangeness, such as the matter created in particle colliders like RHIC and LHC and determined the ranges that can be probed (given specific initial conditions) by charge and isospin chemical potentials during deconfinement.

Unlike quark matter produced in the lab, quark matter created inside stars can be strange, as the timeframe for its creation is much longer than the timeframe for

weak decay. To discuss the effects of net strangeness on deconfinement to quark matter, we have constructed 2-dimensional phase diagrams at two chosen temperatures of $T = 0$ and $T = 160$ MeV. In the former case, very little strangeness is created and, therefore, its effects are minimal. In the latter, the consequences of nonzero strangeness are significant.

At zero temperature, we have found that, for non-strange matter ($Y_S = 0$), μ_Q and μ_I cover a range from -420 to 0 MeV, reaching more negative values on the hadronic side of the phase transition. For the strange case $Y_S \neq 0$, the corresponding range is -320 to 0 MeV, once again reaching more negative values on the hadronic side of the phase transition. On the quark side of the phase transition, μ_Q and μ_I lie between -75 and 0 MeV. At large temperatures close to the critical point, μ_Q and μ_I become practically the same on the hadronic and the quark sides and have intermediate values for $Y_S = 0$ ranging from -110 to 0 MeV. Finally, when strangeness is allowed, μ_Q and μ_I at large temperature become less negative and even positive, reaching ~ 50 MeV.

ACKNOWLEDGEMENTS

We acknowledge the colleagues Jeffrey Peterson and Michael Strickland for valuable suggestions. Support for this research comes from the National Science Foundation under grant PHY-1748621, PHAROS (COST Action CA16214), the LOEWE-Program in HIC for FAIR, Conselho Nacional de Desenvolvimento Científico e Tecnológico - CNPq under grant 304758/2017-5 (R.L.S.F.), and Fundação de Amparo à Pesquisa do Estado do Rio Grande do Sul - FAPERGS under grants 19/2551-0000690-0 and 19/2551-0001948-3 (R.L.S.F.).

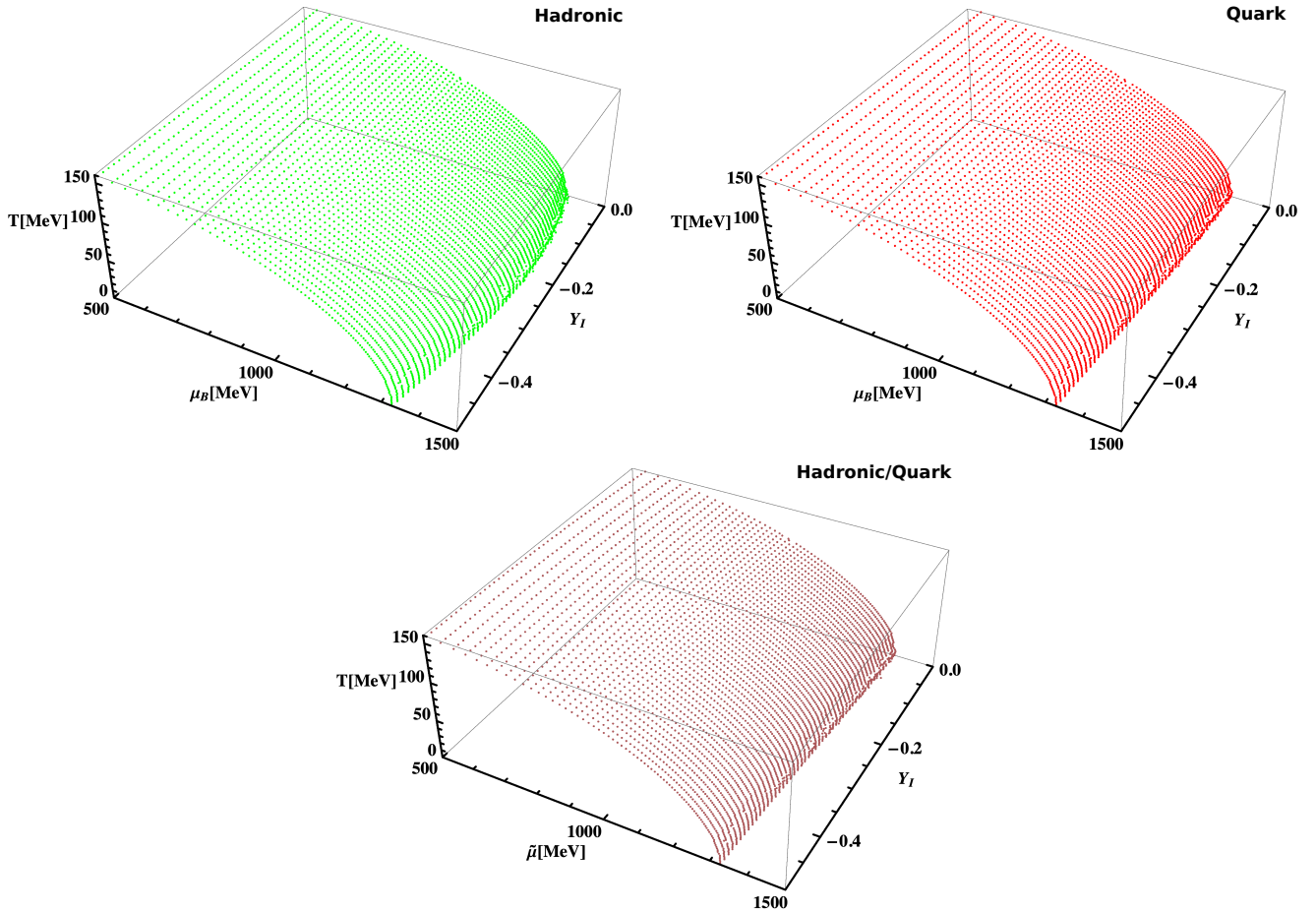


Fig. A1: Same as Fig. 1 but showing the isospin charge fraction Y_I .

Particle	Q_B	Q	Q_S	Q_I
p	1	1	0	$1/2$
n	1	0	0	$-1/2$
Λ	1	0	1	0
Σ^+	1	1	1	1
Σ^0	1	0	1	0
Σ^-	1	-1	1	-1
Ξ^0	1	0	2	$-3/2$
Ξ^-	1	-1	2	$-1/2$
u	$1/3$	$2/3$	0	$1/2$
d	$1/3$	$-1/3$	0	$-1/2$
s	$1/3$	$-1/3$	1	0

TABLE A1: Baryon number Q_B , electric charge Q , strangeness Q_S , and isospin Q_I for the baryon octet and the three light quarks. Antiparticles carry opposite signs.

APPENDIX A

The chemical potentials of the various baryon and quark species are obtained using the appropriate values

from Table I in conjunction with Eq. 5:

$$\begin{aligned}
 \mu_p &= \mu_B + \mu_Q, \\
 \mu_n &= \mu_B, \\
 \mu_\Lambda &= \mu_B + \mu_S, \\
 \mu_\Sigma^+ &= \mu_B + \mu_Q + \mu_S, \\
 \mu_\Sigma^0 &= \mu_B + \mu_S, \\
 \mu_\Sigma^- &= \mu_B - \mu_Q + \mu_S, \\
 \mu_\Xi^0 &= \mu_B + 2\mu_S, \\
 \mu_\Xi^- &= \mu_B - \mu_Q + 2\mu_S,
 \end{aligned} \tag{A1}$$

$$\begin{aligned}
 \mu_u &= \frac{1}{3}\mu_B + \frac{2}{3}\mu_Q, \\
 \mu_d &= \frac{1}{3}\mu_B - \frac{1}{3}\mu_Q, \\
 \mu_s &= \frac{1}{3}\mu_B - \frac{1}{3}\mu_Q + \mu_S.
 \end{aligned} \tag{A2}$$

Once more, we remind the reader that we consider the strangeness of particles to be positive in our notation. Otherwise, all $Q_{S,i}$, n_S , and Y_S would have to be multiplied by -1 . This would also reverse the sign of μ_S in all equations. In the equivalent isospin formalism discussed

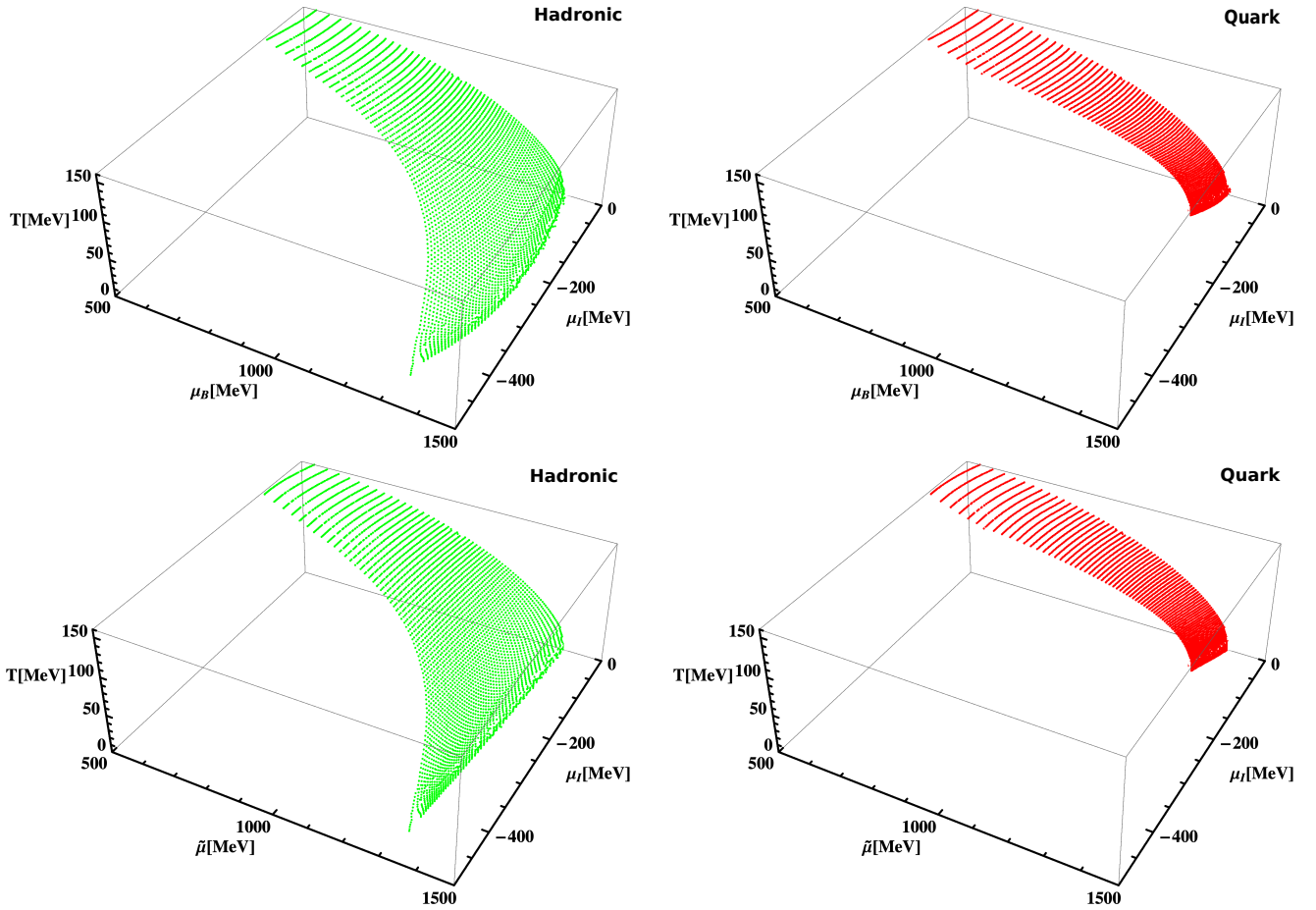


Fig. A2: Same as Fig. 2 but showing the isospin chemical potential μ_I .

in Section II B, the chemical potentials for the different species look the same, except for μ_Q being replaced by μ_I . This can be obtained by replacing the values of $Q_{B,i}$, $Q_{I,i}$ and $Q_{S,i}$ for each baryonic or quark species in Eq. (11).

APPENDIX B

For the purposes of extending the discussion of Section III A to the equivalent isospin formalism, we present Figs. A1 and A2, where we plot phase diagrams in terms

of the isospin fraction Y_I and isospin chemical potential μ_I (as opposed to the earlier Y_Q and μ_Q). Since for non-strange matter Eq. (10) reduces simply to $Y_I = Y_Q - 0.5$, Fig. A1 is very similar to Fig. 1, only differing by the 0.5 shift in the Y_I axis.

Fig. A2 is exactly like Fig. 2, which is a consequence of the middle term being the same in Eq. (13) and Eq. (15) in order to reproduce the same particle chemical potential expressions of Appendix A. All of the statements made in this Appendix and in the end of Section III B were verified numerically by rewriting our numerical code to run for fixed isospin fractions.

[1] M. Hanuske, J. Steinheimer, L. Bovard, A. Mukherjee, S. Schramm, K. Takami, J. Papenfort, N. Wechselberger, L. Rezzolla, and H. Stöcker, *Proceedings, Workshop on Discovery Physics at the LHC (Kruger2016): Kruger National Park, Mpumalanga, South Africa, December 5-9, 2016*, J. Phys. Conf. Ser. **878**, 012031 (2017).

[2] N.-U. F. Bastian, D. Blaschke, T. Fischer, and G. Röpke, Universe **4**, 67 (2018), arXiv:1804.10178 [nucl-th].

[3] A. Burrows and J. M. Lattimer, *Astrophys. J.* **307**, 178 (1986).

[4] J. A. Pons, S. Reddy, M. Prakash, J. M. Lattimer, and J. A. Miralles, *Astrophys. J.* **513**, 780 (1999), arXiv:astro-ph/9807040 [astro-ph].

[5] F. Galeazzi, W. Kastaun, L. Rezzolla, and J. A. Font, *Phys. Rev.* **D88**, 064009 (2013), arXiv:1306.4953 [gr-qc].

[6] A. Perego, S. Bernuzzi, and D. Radice, *Eur. Phys. J. A* **55**, 124 (2019), arXiv:1903.07898 [gr-qc].

[7] E. R. Most, L. J. Papenfort, V. Dexheimer, M. Hanuske, H. Stöcker, and L. Rezzolla, (2019), arXiv:1910.13893 [astro-ph.HE].

[8] L. Hudepohl, B. Muller, H. T. Janka, A. Marek, and G. G. Raffelt, *Phys. Rev. Lett.* **104**, 251101 (2010), [Erratum: *Phys. Rev. Lett.* 105, 249901 (2010)], arXiv:0912.0260 [astro-ph.SR].

[9] T. Fischer, S. C. Whitehouse, A. Mezzacappa, F. K. Thielemann, and M. Liebendorfer, *Astron. Astrophys.* **517**, A80 (2010), arXiv:0908.1871 [astro-ph.HE].

[10] M. Martinez, M. D. Sievert, D. E. Wertepny, and J. Noronha-Hostler, (2019), arXiv:1911.10272 [nucl-th].

[11] F. Karsch, *Lectures on quark matter. Proceedings, 40. International Universit tswochen for theoretical physics, 40th Winter School, IUKT 40: Schladming, Austria, March 3-10, 2001*, *Lect. Notes Phys.* **583**, 209 (2002), arXiv:hep-lat/0106019 [hep-lat].

[12] S. Muroya, A. Nakamura, C. Nonaka, and T. Takaishi, *Prog. Theor. Phys.* **110**, 615 (2003), arXiv:hep-lat/0306031 [hep-lat].

[13] P. F. Bedaque, *Proceedings, 35th International Symposium on Lattice Field Theory (Lattice 2017): Granada, Spain, June 18-24, 2017*, *EPJ Web Conf.* **175**, 01020 (2018), arXiv:1711.05868 [hep-lat].

[14] B.-A. Li, C. M. Ko, and W. Bauer, *International Journal of Modern Physics E* **07**, 147D229 (1998).

[15] A. B. Migdal, E. E. Saperstein, M. A. Troitsky, and D. N. Voskresensky, *Phys. Rept.* **192**, 179 (1990).

[16] A. Steiner, M. Prakash, J. Lattimer, and P. Ellis, *Physics Reports* **411**, 325D375 (2005).

[17] B. B. Brandt, G. Endr di, E. S. Fraga, M. Hippert, J. Schaffner-Bielich, and S. Schmalzbauer, *Phys. Rev. D* **98**, 094510 (2018).

[18] D. J. Schwarz and M. Stuke, *Journal of Cosmology and Astroparticle Physics* **2009**, 025 (2009).

[19] S. Cotter, P. Giudice, S. Hands, and J.-I. Skulderud, *Phys. Rev. D* **87**, 034507 (2013), arXiv:1210.4496 [hep-lat].

[20] V. V. Braguta, E. M. Ilgenfritz, A. Yu. Kotov, A. V. Molochkov, and A. A. Nikolaev, *Phys. Rev. D* **94**, 114510 (2016), arXiv:1605.04090 [hep-lat].

[21] G. S. Bali, F. Bruckmann, G. Endrodi, Z. Fodor, S. D. Katz, and A. Schafer, *Phys. Rev. D* **86**, 071502 (2012), arXiv:1206.4205 [hep-lat].

[22] G. S. Bali, F. Bruckmann, G. Endrodi, Z. Fodor, S. D. Katz, S. Krieg, A. Schafer, and K. K. Szabo, *JHEP* **02**, 044 (2012), arXiv:1111.4956 [hep-lat].

[23] G. S. Bali, F. Bruckmann, G. Endr di, S. D. Katz, and A. Sch fer, *JHEP* **08**, 177 (2014), arXiv:1406.0269 [hep-lat].

[24] V. V. Braguta, V. A. Goy, E. M. Ilgenfritz, A. Yu. Kotov, A. V. Molochkov, M. Muller-Preussker, and B. Petersson, *JHEP* **06**, 094 (2015), arXiv:1503.06670 [hep-lat].

[25] V. V. Braguta, E. M. Ilgenfritz, A. Yu. Kotov, B. Petersson, and S. A. Skinderev, *Phys. Rev. D* **93**, 034509 (2016), arXiv:1512.05873 [hep-lat].

[26] J. B. Kogut and D. K. Sinclair, *Phys. Rev. D* **66**, 034505 (2002).

[27] J. B. Kogut and D. K. Sinclair, *Phys. Rev. D* **66**, 014508 (2002).

[28] D. T. Son and M. A. Stephanov, *Phys. Rev. Lett.* **86**, 592 (2001).

[29] D. T. Son and M. A. Stephanov, *Phys. Atom. Nucl.* **64**, 834 (2001), [Yad. Fiz. 64, 899 (2001)], arXiv:hep-ph/0011365 [hep-ph].

[30] L. Lepori and M. Mannarelli, *Phys. Rev. D* **99**, 096011 (2019).

[31] S. Carignano, L. Lepori, A. Mammarella, M. Mannarelli, and G. Pagliaroli, *Eur. Phys. J. A* **53**, 35 (2017), arXiv:1610.06097 [hep-ph].

[32] O. Janssen, M. Kieburg, K. Splittorff, J. J. M. Verbaarschot, and S. Zafeiropoulos, *Phys. Rev. D* **93**, 094502 (2016).

[33] T. D. Cohen and S. Sen, *Nucl. Phys.* **A942**, 39 (2015), arXiv:1503.00006 [hep-ph].

[34] E. S. Fraga, L. F. Palhares, and C. Villavicencio, *Phys. Rev. D* **79**, 014021 (2009).

[35] M. Loewe and C. Villavicencio, *Phys. Rev. D* **67**, 074034 (2003).

[36] M. Loewe and C. Villavicencio, *Phys. Rev. D* **71**, 094001 (2005).

[37] K. Splittorff, D. T. Son, and M. A. Stephanov, *Phys. Rev. D* **64**, 016003 (2001).

[38] M. Mannarelli, *Particles* **2**, 411 (2019), arXiv:1908.02042 [hep-ph].

[39] T. G. Khunjua, K. G. Klimenko, R. N. Zhokhov, and V. C. Zhukovsky, *Phys. Rev. D* **95**, 105010 (2017).

[40] T. G. Khunjua, K. G. Klimenko, and R. N. Zhokhov, *Phys. Rev. D* **98**, 054030 (2018).

[41] T. G. Khunjua, K. G. Klimenko, and R. N. Zhokhov, *Eur. Phys. J. C* **79**, 151 (2019), arXiv:1812.00772 [hep-ph].

[42] T. Xia, L. He, and P. Zhuang, *Phys. Rev. D* **88**, 056013 (2013).

[43] C.-f. Mu, L.-y. He, and Y.-x. Liu, *Phys. Rev. D* **82**, 056006 (2010).

[44] H. Abuki, R. Anglani, R. Gatto, M. Pellicoro, and M. Ruggieri, *Phys. Rev. D* **79**, 034032 (2009).

[45] J. O. Andersen and L. T. Kyllingstad, *Journal of Physics G: Nuclear and Particle Physics* **37**, 015003 (2009).

[46] G. Sun, L. He, and P. Zhuang, *Phys. Rev. D* **75**, 096004 (2007).

[47] D. Ebert and K. G. Klimenko, *Eur. Phys. J. C* **46**, 771 (2006), arXiv:hep-ph/0510222 [hep-ph].

[48] D. Ebert and K. G. Klimenko, *Journal of Physics G: Nuclear and Particle Physics* **32**, 599 (2006).

[49] L. He, M. Jin, and P. Zhuang, *Phys. Rev. D* **74**, 036005 (2006).

[50] L. He, M. Jin, and P. Zhuang, *Phys. Rev. D* **71**, 116001 (2005).

[51] L. He and P. Zhuang, *Phys. Lett. B* **615**, 93 (2005), arXiv:hep-ph/0501024 [hep-ph].

[52] A. Barducci, R. Casalbuoni, G. Pettini, and L. Ravagli, *Phys. Rev. D* **69**, 096004 (2004).

[53] D. Toublan and J. B. Kogut, *Phys. Lett. B* **564**, 212 (2003), arXiv:hep-ph/0301183 [hep-ph].

[54] M. Frank, M. Buballa, and M. Oertel, *Phys. Lett. B* **562**, 221 (2003), arXiv:hep-ph/0303109 [hep-ph].

[55] S. Mukherjee, M. G. Mustafa, and R. Ray, *Phys. Rev. D* **75**, 094015 (2007).

[56] A. Bhattacharyya, S. K. Ghosh, A. Lahiri, S. Majumder, S. Raha, and R. Ray, *Phys. Rev. C* **89**, 064905 (2014).

[57] J. O. Andersen, N. Haque, M. G. Mustafa, and M. Strickland, *Phys. Rev. D* **93**, 054045 (2016),

arXiv:1511.04660 [hep-ph].

[58] P. Adhikari, J. O. Andersen, and P. Kneschke, Phys. Rev. D **98**, 074016 (2018).

[59] R. Stiele, E. S. Fraga, and J. Schaffner-Bielich, Phys. Lett. **B729**, 72 (2014), arXiv:1307.2851 [hep-ph].

[60] H. Ueda, T. Z. Nakano, A. Ohnishi, M. Ruggieri, and K. Sumiyoshi, Phys. Rev. D **88**, 074006 (2013).

[61] K. Kamikado, N. Strodthoff, L. von Smekal, and J. Wambach, Phys. Lett. **B718**, 1044 (2013), arXiv:1207.0400 [hep-ph].

[62] A. Parnachev, JHEP **02**, 062 (2008), arXiv:0708.3170 [hep-th].

[63] J. Erdmenger, M. Kaminski, and F. Rust, Phys. Rev. D **77**, 046005 (2008), arXiv:0710.0334 [hep-th].

[64] O. Aharony, K. Peeters, J. Sonnenschein, and M. Zamaklar, JHEP **02**, 071 (2008), arXiv:0709.3948 [hep-th].

[65] A. Rebhan, A. Schmitt, and S. A. Stricker, JHEP **05**, 084 (2009), arXiv:0811.3533 [hep-th].

[66] H. Nishihara and M. Harada, Phys. Rev. D **89**, 076001 (2014).

[67] H. Nishihara and M. Harada, Phys. Rev. D **90**, 115027 (2014), arXiv:1407.7344 [hep-ph].

[68] M. Lv, D. Li, and S. He, JHEP **11**, 026 (2019), arXiv:1811.03828 [hep-ph].

[69] B. B. Brandt, G. Endrodi, and S. Schmalzbauer, Phys. Rev. D **97**, 054514 (2018).

[70] B. B. Brandt, G. Endrodi, and S. Schmalzbauer, *Proceedings, 35th International Symposium on Lattice Field Theory (Lattice 2017): Granada, Spain, June 18-24, 2017*, EPJ Web Conf. **175**, 07020 (2018), arXiv:1709.10487 [hep-lat].

[71] B. B. Brandt and G. Endrodi, *Proceedings, 34th International Symposium on Lattice Field Theory (Lattice 2016): Southampton, UK, July 24-30, 2016*, PoS **LATTICE2016**, 039 (2016), arXiv:1611.06758 [hep-lat].

[72] B. B. Brandt, G. Endrodi, and S. Schmalzbauer, .

[73] P. Adhikari and J. O. Andersen, Phys. Lett. **B804**, 135352 (2020), arXiv:1909.01131 [hep-ph].

[74] P. Adhikari and J. O. Andersen, (2019), arXiv:1909.10575 [hep-ph].

[75] P. Adhikari, J. O. Andersen, and P. Kneschke, Eur. Phys. J. **C79**, 874 (2019), arXiv:1904.03887 [hep-ph].

[76] S. S. Avancini, A. Bandyopadhyay, D. C. Duarte, and R. L. S. Farias, Phys. Rev. **D100**, 116002 (2019), arXiv:1907.09880 [hep-ph].

[77] Z.-Y. Lu, C.-J. Xia, and M. Ruggieri, Eur. Phys. J. **C80**, 46 (2020), arXiv:1907.11497 [hep-ph].

[78] Z.-Q. Wu, Chao-Shi, J.-L. Ping, and H.-S. Zong, (2020), arXiv:2003.02988 [hep-ph].

[79] F. Rennecke, W.-j. Fu, and J. M. Pawłowski, *Proceedings, 18th Hellenic School and Workshops on Elementary Particle Physics and Gravity (CORFU2018): Corfu, Corfu, Greece*, PoS **CORFU2018**, 182 (2019), arXiv:1907.08179 [hep-ph].

[80] K. Lee, M. Rhoades-Brown, and U. W. Heinz, Phys. Lett. B **174**, 123 (1986).

[81] U. W. Heinz, K. S. Lee, and M. J. Rhoades-Brown, Mod. Phys. Lett. **A2**, 153 (1987).

[82] P. Koch, J. Rafelski, and W. Greiner, Phys. Lett. B **123**, 151 (1983).

[83] B. Lukacs, J. Zimanyi, and N. Balazs, Phys. Lett. B **183**, 27 (1987).

[84] C. Bonati, M. D'Elia, M. Mariti, M. Mesiti, F. Negro, and F. Sanfilippo, Phys. Rev. **D92**, 054503 (2015), arXiv:1507.03571 [hep-lat].

[85] S. Borsanyi, Z. Fodor, J. N. Guenther, R. Kara, S. D. Katz, P. Parotto, A. Pasztor, C. Ratti, and K. K. Szabo, (2020), arXiv:2002.02821 [hep-lat].

[86] A. Monnai, B. Schenke, and C. Shen, Phys. Rev. **C100**, 024907 (2019), arXiv:1902.05095 [nucl-th].

[87] J. Steinheimer, S. Schramm, and H. Stocker, Phys. Rev. **C84**, 045208 (2011), arXiv:1108.2596 [hep-ph].

[88] A. Motornenko, J. Steinheimer, V. Vovchenko, S. Schramm, and H. Stoecker, Phys. Rev. **C101**, 034904 (2020), arXiv:1905.00866 [hep-ph].

[89] V. Dexheimer and S. Schramm, Astrophys. J. **683**, 943 (2008), arXiv:0802.1999 [astro-ph].

[90] V. A. Dexheimer and S. Schramm, Phys. Rev. **C81**, 045201 (2010), arXiv:0901.1748 [astro-ph.SR].

[91] C. Ratti, M. A. Thaler, and W. Weise, *Proceedings, 18th International Conference on Ultra-Relativistic Nucleus-Nucleus Collisions (Quark Matter 2005): Budapest, Hungary, August 4-9, 2005*, Rom. Rep. Phys. **58**, 13 (2006).

[92] S. Roessner, C. Ratti, and W. Weise, Phys. Rev. **D75**, 034007 (2007), arXiv:hep-ph/0609281 [hep-ph].

[93] J. Roark and V. Dexheimer, Phys. Rev. **C98**, 055805 (2018), arXiv:1803.02411 [nucl-th].

[94] C. Ratti, M. A. Thaler, and W. Weise, Phys. Rev. **D73**, 014019 (2006), arXiv:hep-ph/0506234 [hep-ph].

[95] Z. Fodor and S. D. Katz, JHEP **04**, 050 (2004), arXiv:hep-lat/0402006 [hep-lat].

[96] V. Dexheimer, R. de Oliveira Gomes, S. Schramm, and H. Pais, J. Phys. G **46**, 034002 (2019), arXiv:1810.06109 [nucl-th].

[97] Y. Aoki, G. Endrodi, Z. Fodor, S. D. Katz, and K. K. Szabo, Nature **443**, 675 (2006), arXiv:hep-lat/0611014 [hep-lat].

[98] “Compose website,” <https://compose.obspm.fr/>.

[99] V. Dexheimer, (2017), 10.1017/pasa.2017.61, arXiv:1708.08342 [astro-ph.HE].

[100] M. Gell-Mann, Nuovo Cim. **4**, 848 (1956).

[101] M. Hempel, V. Dexheimer, S. Schramm, and I. Iosilevskiy, Phys. Rev. **C88**, 014906 (2013), arXiv:1302.2835 [nucl-th].